4. D. S. Broomhead and G. P. King, *Phys. D* **20**, 217 (1986).
5. M. P. Chauve and P. LeGal, *ibid.* **58**, 407 (1992).
6. J. L. Lumley, in (*3*), pp. 105–122.
7. N. Aubry *et al.*, *J. Fluid Mech.* **192**, 115 (1988).
8. A. Glezer, Z. Kadioglu, A. J. Pearlstein, *Phys. Fluids A* **1**, 1363 (1989).
9. Y. Takeda, *Nucl. Eng. Des.* **126**, 277 (1990).
10. R. C. DiPrima and H. L. Swinney, in *Hydrodynamic Instabilities and the Transition to Turbulence*, H. L. Swinney and J. P. Gollub, Eds. (Springer-Verlag, Berlin, 1985), pp. 139–180.
11. P. R. Fenstermacher, H. L. Swinney, J. P. Gollub, *J. Fluid Mech.* **94**, 103 (1979).
12. M. Gorman and H. L. Swinney, *ibid.* **117**, 123 (1982).
13. L. H. Zhang and H. L. Swinney, *Phys. Rev. A* **31**, 1006 (1985).
14. P. S. Marcus, *J. Fluid Mech.* **146**, 65 (1984).
15. K. T. Coughlin and P. S. Marcus, *ibid.* **234**, 1 (1992); *ibid.*, p. 19.
16. ______, R. P. Tagg, H. L. Swinney, *Phys. Rev. Lett.* **66**, 1161 (1991).
17. Y. Takeda, K. Kobayashi, W. E. Fischer, *Exp. Fluids* **9**, 317 (1990).
18. Y. Takeda, W. E. Fischer, K. Kobayashi, T. Takada, *ibid.* **13**, 199 (1992).
19. Y. Takeda, W. E. Fischer, J. Sakakibara, K. Ohmura, *Phys. Rev. E* **47**, 4130 (1993).
20. Y. Takeda, W. E. Fischer, J. Sakakibara, *Phys. Rev. Lett.* **70**, 3569 (1993).
21. D. Andereck, S. S. Liu, H. L. Swinney, *J. Fluid Mech.* **164**, 155 (1986).
22. R. Tagg *et al.*, *Phys. Rev. A* **39**, 3734 (1989).

3 August 1993; accepted 30 November 1993

Constraints on Transport and Kinetics in Hydrothermal Systems from Zoned Garnet Crystals

Bjørn Jamtveit* and Richard L. Hervig

Zonation of oxygen isotope ratios, fluorine, and rare earth element abundances across garnet crystals from the Permian Oslo Rift reflect temporal variation of the hydrothermal system in which the garnets grew. A sharp rimward decrease in the $^{18}O/^{16}O$ ratio (of 5 per mil) across the interface between aluminum-rich garnet cores and iron-rich rims indicates influx of meteoric fluids to a system initially dominated by magmatic fluids. This influx may record the transition from ductile to brittle deformation of the hydrothermally altered rocks. In contrast, fluorine and light rare earth element concentrations increase at the core-rim interface. These data may reflect enhanced advective transport and notable kinetic control on trace element uptake by the garnets during brittle deformation.

Hydrothermal systems play a key role in the chemical differentiation of the Earth's crust. The understanding of such systems requires integrated studies of active as well as ancient systems. Ancient systems contain the integrated results of hydrothermal activity occurring at depths that are inaccessible to direct observations. The main problem when studying ancient systems is to determine their temporal evolution. Analysis of intracrystalline zonation of hydrothermal minerals may provide a more or less continuous record of the processes taking place during the evolution of ancient hydrothermal systems (*1*). Such data are needed to test and complement results obtained from theoretical models of hydrothermal system dynamics. Here, we present ion microprobe analyses (IMPA) of zoned hydrothermal garnets from the Permian Oslo Rift, Norway, which provide information on the sources of hydrothermal fluids, their compositional evolution, and the extent and mechanism of mass transfer between fluids and the rock matrix.

The garnets that we studied are representative of a large population of hydrothermal garnets from layered shale-carbonate rock sequences in the contact aureole of the Drammen granite (*1*). These rocks were infiltrated by fluids during cooling of the granite. Early infiltration was pervasive and coeval with more or less ductile deformation, whereas later infiltration was focused along faults and fractures formed during brittle deformation (*1, 2–4*). Garnets grew throughout these events. Mineral equilibria and fluid inclusion results indicate that the garnets formed at temperatures of 350°C to 400°C. Backscattered electron (BSE) images (Fig. 1) show a sharp transition from a relatively grossular-rich core (gr = 20 to 40 mol%) to an andradite-rich rim (gr <5 mol%). The rim furthermore contains several thin layers of more grossular-rich composition that give rise to the oscillatory zonation pattern evident in the BSE image (Fig. 1). The composition of the grossular-rich layers was largely determined by the local mineral assemblage during periods of slow fluid influx and low crystal growth rates, whereas the composition of more rapidly grown (*5*) andradite-rich layers reflects infiltration of externally derived hydrothermal fluids with high concentrations of As and W (*1, 6*). The andradite-rich garnets are extremely low in high–field strength elements (HFEs) such as Zr, Y, and Ti. The lack of evidence that local sources of HFEs (notably zircon and sphene) were removed from the system indicates that the fluids did not reach equilibrium concentrations with respect to these components during growth of the andradite-rich rims. Thus, models of fluid flow and chemical reaction kinetics in hydrothermal systems that assume local fluid-rock equilibrium may not always be valid (*7*). To obtain more detailed information about the mass transport, mass transfer, kinetic dispersion, aqueous complexation, and the fluid sources, we analyzed the garnet shown in Fig. 1 for oxygen isotope, fluorine, and rare earth element (REE) compositions.

The oxygen isotope zonation profile (Fig. 2A) reveals a marked discontinuity at the core-rim interface, suggesting that the pore fluid had a relatively higher oxygen isotope ratio when the garnet core was growing. Fractionation factors for the garnet-H_2O system at 350°C, corrected for compositional variations of the garnet (*8, 9*), indicate that the core and rim precipitated from fluids with average $\delta^{18}O$ values [relative to standard mean ocean water (SMOW)] of +10 per mil and +6 per mil, respectively. A value of +10 per mil is that expected for fluid equilibrated with the Drammen granite at high temperature (*4*), whereas the value of +6 per mil may indicate an appreciable meteoric water component in the hydrothermal fluid [the oxygen composition of Permian meteoric water in this area was probably around −12 per mil (*10*)].

Additional information on changes in the hydrothermal system is provided by F and REE data from the garnet. Considerable amounts of F may substitute for OH

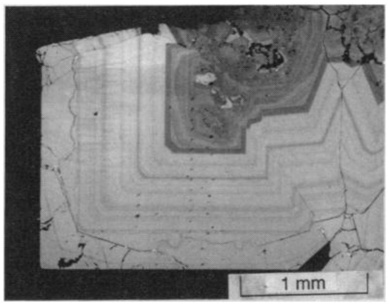

Fig. 1. Backscattered electron image of a dodecahedral garnet crystal selected for ion microprobe analysis. The garnet is essentially a binary solution between the end members grossular (gr = $Ca_3Al_2Si_3O_{12}$) and andradite (and = $Ca_3Fe_2Si_3O_{12}$). The image shows andradite-rich garnet (light color) growing on grossular-richer core (dark). Oscillatory zonation seen in andradite-rich rim reflects different relative proportions of major components andradite and grossular. Dark spots show the sites of oxygen isotope analyses.

B. Jamtveit, Department of Geology, University of Oslo, Post Office Box 1047 Blindern, N-0316 Oslo, Norway.
Richard L. Hervig, Center for Solid State Science, Arizona State University, Tempe, AZ 85287.

*To whom correspondence should be addressed.

that is invariably present in hydrothermal garnets (*11*). The F content of our sample (Fig. 2B) increases abruptly at the core-rim boundary and reaches values near 6000 parts per million in the rim. The outermost margin (0 to 300 μm from the edge) is, however, generally poor in F.

Except for the outermost margin, the garnet rim is enriched in the light REEs (LREEs) relative to the core (Fig. 3) as well as in As, W, Mo, and Fe and is relatively depleted in Zr, Y, Ti, and Al (*1*). Lanthanum shows the most abrupt increase at the 900-μm boundary, followed by Ce and then Nd. The outermost margin is low in REEs as well as in As, W, and Mo (*1*). The grossular-rich garnets, including the garnet cores, are typically depleted in LREE as compared to the abundance in the host rock, whereas the concentration of Sm and heavier REEs is comparable to those of the host rock (Fig. 4). A small, but significant, positive Eu anomaly is evident in most samples. In contrast, the andradite rims are strongly enriched in the LREEs. However, there is a notable La depletion relative to the other LREE in the most LREE-rich samples. The rims are furthermore depleted in the HREE and show a distinct positive Eu anomaly. Although the andradite-rich garnets have a wide range in REE concentrations, the chondrite-normalized patterns are broadly similar. The outermost garnet margins have flat or slightly LREE-depleted REE patterns (Fig. 4).

Neodymium isotope data from these garnets demonstrate that the elevated LREE concentrations observed in the garnet rims (Fig. 3) are associated with the supply of REE from the magmatic system (Fig. 5).

The correlation between the contents of trace components derived from the magmatic system in the zoned garnets, as well as a marked similarity among the zonation patterns of different garnet crystals from the same sample (*6*), indicate that the zonation patterns are to a large extent controlled by large-scale transport processes. In such a case, the garnet composition may vary as a result of variations in the composition of the bulk pore fluid at the site of crystal growth or as a result of a change in the mechanism by which trace elements are taken up by the garnet during crystal growth. The local pore fluid composition is affected by the competition between local buffering and external controls through infiltrating fluids. Fluctuations in the concentration of some externally derived component in the pore fluid at the site of crystal growth may indicate a change in the advective transport rate or a change in the concentration of this component at the fluid inlet. In a flow system with finite kinetic dispersion, advective mass transport may affect the local pore-fluid composition to different extents for different components as a result of differences in the fluid-rock partitioning (*12*). Thus, rapidly transported components may be completely externally controlled, whereas others are locally buffered.

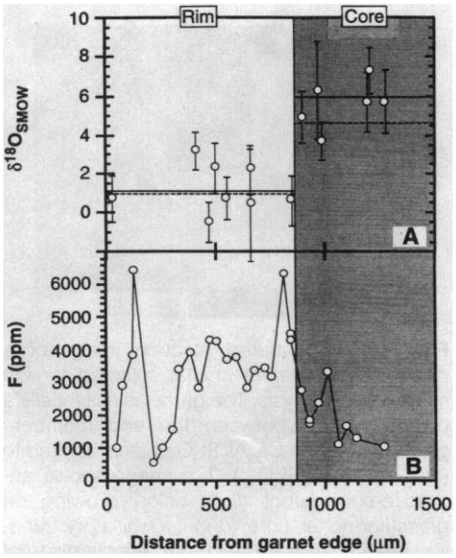

Fig. 2. (**A**) Oxygen isotope zonation profile of garnet shown in Fig. 1 (*19*). (**B**) Fluorine zonation profile across garnet shown in Fig. 1 (*20*).

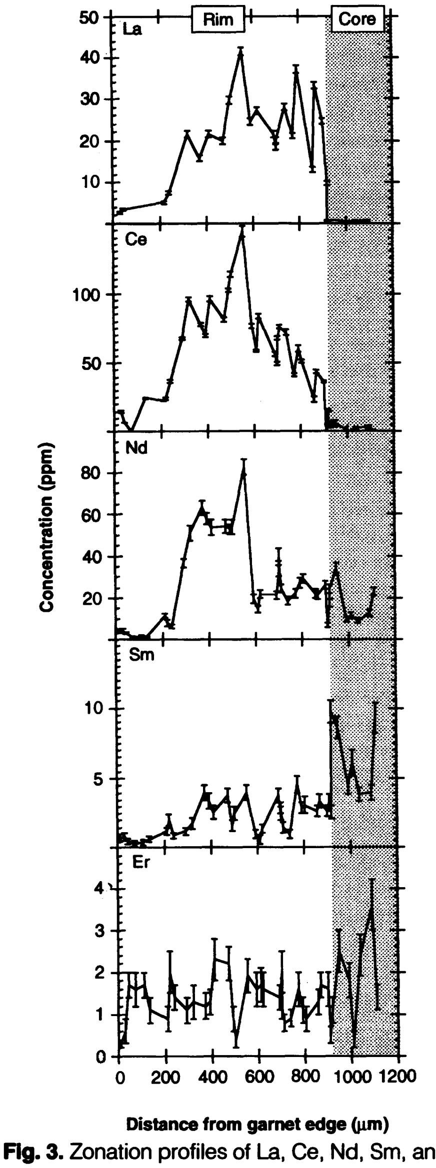

Fig. 3. Zonation profiles of La, Ce, Nd, Sm, and Er across the garnet shown in Fig. 1 (*21*).

The oxygen isotope results imply that the isotope signature of the garnet was externally controlled during all stages of garnet crystallization [as suggested in (*4*)]. Influx of fluids with an appreciable meteoric component during garnet rim growth would imply that the fluid pressure at this stage approached hydrostatic values and thus that a connected porosity had formed from the site of crystal growth toward the near-surface environment. The formation of a connected porosity was probably associated with extensive brittle deformation near the granite roof (*2*), and an accompanying increase in rock permeability may have allowed a marked increase in the fluid flow rates. Increased flow rate would result in enhanced advective transport rates and kinetic dispersion and may have resulted in increased infiltration control on the pore-fluid composition for a wide range of com-

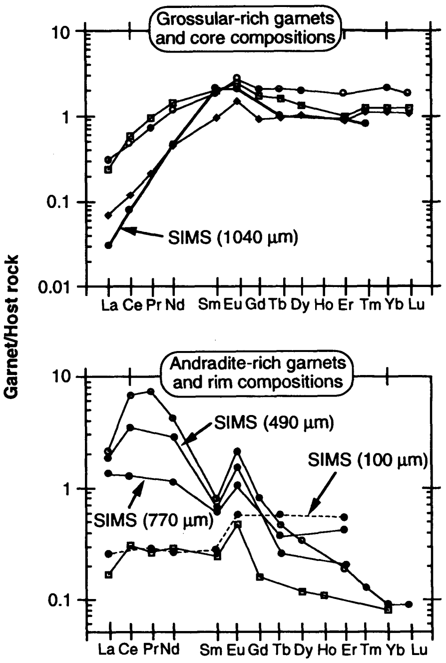

Fig. 4. Chondrite-normalized REE patterns showing typical garnet core and rim compositions (closed circles). Additional IMPA, some of which are depicted here, include Eu and Tb. Distances are as in Fig. 2. ICP-MS analyses of bulk garnet separates are also given (open symbols). The ICP-MS analyses were done at the Department of Geology, University of Bristol, according to the methods described by Kemp (*22*).

ponents during andradite precipitation.

The "magmatic" oxygen isotope composition of grossular-rich garnet cores coupled with a Nd isotope composition indicative of a sedimentary source (Fig. 5) probably indicate that the advective transport rate of REEs is much lower than that of oxygen at moderate fluid flow rates where the extent of kinetic dispersion is limited. Thus, the garnet core grew downstream of the Nd isotope front but upstream of the oxygen isotope front. The LREE depletion of the cores shows that the relatively smaller HREE fits better into the eightfold coordination site of the garnet lattice than the larger LREE (*13*).

The Nd isotope composition of the rims, in contrast to that of the core, indicates an appreciable input of Nd derived from the magmatic system. Furthermore, there is a continuous change from sedimentary to magmatic Nd isotope signatures (Fig. 5), indicating that there are no sharp Nd isotope fronts. Thus, we suggest that at this stage the fluid flow rate is high enough to cause extensive kinetic dispersion. As the kinetic dispersion increases, the advective transport rates of oxygen and Nd would converge (*12*). This explains the infiltration control on oxygen as well as on Nd isotope signatures for the rim. Thus, it seems that the differences between the core and rim REE compositions were, at least partly, a result of variable advective transport rates. Furthermore, differential transport rates of the REE are indicated by the abrupt increase in La concentration immediately at the core-rim boundary; this buildup indicates that La was transported more rapidly than Ce and Nd. Because HREEs are compatible in garnet, the low HREE content of the garnet rim shows that the pore fluid must have been depleted in HREE. The most likely explanation for this is higher retardation of the HREE as compared with the LREE along the flow path, possibly as a result of preferential incorporation of HREE into garnet or other phases upstream of the analyzed crystal.

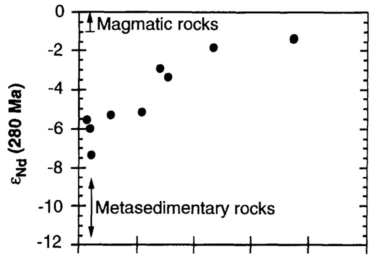

Fig. 5. Neodymium concentration (*23*) versus ε_{Nd} values calculated at 280 Ma (estimated age of the Drammen granite) for bulk garnet separates. The positive correlation observed indicates supply of Nd from the magmatic system during garnet growth. The age of the Drammen granite and the ranges in ε_{Nd} for the Drammen granite and the host metasedimentary rocks are from Trønnes and Brandon (*14*) and Jamtveit (*24*).

The oxygen isotope signature for the rim indicates an appreciable contribution from meteoric fluids at this stage. However, the meteoric contribution required to lower the hydrothermal fluid composition from a magmatic value of +10 per mil to +6 per mil (about 20%) would not cause major dilution of the components derived from the magmatic system.

The extreme LREE enrichment observed for the garnet rims as well as the positive Eu anomalies are hard to explain by equilibrium partitioning of REE between the hydrothermal fluids and the garnet lattice. In fact, the rim REE patterns are qualitatively similar to REE patterns from acidic, high-temperature hydrothermal fluids (*15–17*). Therefore, we speculate that the rim REE composition may to a large extent have been controlled by irreversible incorporation of REE initially adsorbed on the garnet surface during periods of rapid crystal growth (*5*). In such a case, the rim REE pattern would reflect surface-fluid REE partitioning rather than bulk lattice control. If correct, this model could explain the La (and Ce) depletion observed for the most LREE-rich garnets as the effect of bulk lattice control on the REE uptake superimposed on the surface control.

The positive correlation between the F and the LREE (notably the La) contents furthermore suggests that F may have been an important complexing agent for REE in the hydrothermal solution. This is in agreement with recent models for REE complexation in aqueous solutions at high temperatures (*18*), and thus the REE fractionation between the garnet surface and the hydrothermal fluid may have been partly controlled by the relative stability of REE fluoro-complexes in the aqueous solution at the ambient conditions.

The low REE contents of the garnet margin may reflect a decrease in garnet growth rate with an associated decrease in the interface controls on the REE uptake. A decrease in growth rate during growth of the outermost rim has been inferred from the morphological evolution of these skarn garnets (*5*). Alternatively, it may simply reflect depletion of LREE in the hydrothermal fluid.

The time series information contained in the garnet zonation profiles provides a detailed record of the geochemical evolution of the present hydrothermal system and constrains the effects of transport and reaction kinetics during fluid-rock interactions.

REFERENCES AND NOTES

1. B. Jamtveit, R. A. Wogelius, D. G. Fraser, *Geology* **21**, 113 (1993).
2. P. M. Ihlen, *Sver. Geol. Unders. Ser. C* **59**, 6 (1986).
3. ———, R. Trønnes, F. M. Vokes, in *Metallization Associated with Acid Magmatism*, A. M. Evans, Ed. (Wiley, London, 1982), pp. 111–136.
4. B. Jamtveit, H. F. Grorud, K. Bucher-Nurminen, *Earth Planet. Sci. Lett.* **114**, 131 (1992).
5. B. Jamtveit and T. B. Andersen, *Phys. Chem. Minerals* **19**, 176 (1992).
6. B. Jamtveit, K. V. Ragnarsdottir, B. J. Wood, in preparation.
7. A. C. Lasaga and D. M. Rye, *Am. J. Sci.* **293**, 361 (1993).
8. U. Lichtenstein and S. Hoernes, *Eur. J. Mineral.* **4**, 239 (1992).
9. B. E. Taylor and J. R. O'Neil, *Contrib. Mineral. Petrol.* **64**, 1 (1977).
10. B. Jamtveit and T. Andersen, *Econ. Geol.*, in press.
11. C. E. Manning and D. K. Bird, *Am. Mineral.* **75**, 859 (1990).
12. At local fluid-rock equilibrium, advective (one-dimensional) transport of a tracer occurs as a geochemical front that moves with a velocity (V) approximately given by $V = W\rho_f / K_d\rho_s$, where W is the fluid flux, ρ_f and ρ_s are the fluid and solid densities, respectively, and K_d is the solid-fluid partition coefficient by mass [M. J. Bickle and D. McKenzie, *Contrib. Mineral. Petrol.* **95**, 384 (1987)]. Thus, at a given distance from the fluid inlet the concentration of rapidly transported tracers may be completely controlled by the fluid flow, whereas the concentration of more slowly moving components may be completely controlled by the local mineralogy, depending on the relative positions of the respective geochemical fronts. In contrast, if the rate of fluid-rock interaction is controlled by slow reaction kinetics relative to the fluid flow rate, the geochemical fronts will become broader as a result of kinetic dispersion and may eventually disappear as recognizable fronts. In the limiting case of infinite dispersion, any tracer will travel with the same velocity as the fluid itself [M. J. Bickle, *Am. J. Sci.* **292**, 289 (1992)]. Thus, the relative transport rates of different components converge with increasing fluid flow velocity.
13. C. Pride and G. K. Muecke, *Contrib. Mineral. Petrol.* **76**, 463 (1981).
14. R. G. Trønnes and A. D. Brandon, *ibid.* **109**, 275 (1992).
15. A. Michard and F. Albarede, *Chem. Geol.* **55**, 51 (1986).
16. A. C. Campbell *et al.*, *Nature* **335**, 514 (1988).
17. A. Michard, *Geochim. Cosmochim. Acta* **53**, 745 (1989).
18. S. A. Wood, *Chem. Geol.* **88**, 99 (1990).
19. Oxygen analyses were done on a Cameca IMS 3f ion microprobe equipped with a standard manufacturer-supplied duoplasmatron, an alkali metal ion source constructed in-house [R. T. Lareau and P. Williams, in *Secondary Ion Mass Spectrometry, SIMS V*, A. Benninghoven, R. J. Colton, D. S. Simons, W. Werner, Eds (Springer-Verlag, Berlin, 1986), Series in Chemical Physics, vol. 44, pp. 149–151], and an auxiliary power supply allowing the sample potential to vary in the range of 0 to 5000 V. A 2-nA Cs^+ beam accelerated to +10 kV was focused onto a 30-μm spot on the sample. Sample charging was controlled with the use of a high-current, high-voltage, four-lens electron flood gun mounted on a 2-3/4–inch Conflat flange [R. L. Hervig, P. Williams, R. M. Thomas, S. N. Schauer, I. M. Steele, *Int. J. Mass Spectrom. Ion. Proc.* **120**, 45 (1992)]. The electron gun was aligned to obtain a maximum count rate for ^{16}O secondary ions with initial kinetic energies of 0 to 40 eV. Negative secondary ions were detected at low mass resolution ($m/\Delta m \approx 500$). The 150-μm transfer optics were used with a 750-μm field aperture. To remove the ^{16}OD, $^{16}OH_2$, and ^{17}OH interferences with ^{18}O, we used extreme energy filtering (EEF). It has recently been shown [S. N.

Schauer and P. Williams, *Int. J. Mass. Spectrom. Ion. Proc.* **103**, 21 (1990)] that by collection of only ions ejected from the sample with energies >300 eV, most molecular species, including hydrides, can be effectively eliminated from the secondary ion spectrum to the part per million level. We counted ions with >350 ± 20 eV, which gave ≈4 E5 counts per second for ^{16}O on the garnets in this study. Total analysis time was 45 min. Typically, we used 100 cycles, which resulted in craters 5 to 7 μm deep. The error expected from counting statistics ranged from 1 to 1.2 per mil (1 SD). Actual errors clustered between 1 and 1.6 per mil, and two analyses showed larger errors. We converted raw ratios to absolute values by comparing values with those of several natural mineral standards and by assuming a linear relation between instrumental oxygen isotope fractionation and molecular weight of the sample. Plain horizontal lines give average core and rim compositions, and the dashed horizontal lines on the figure represent the oxygen isotope composition obtained for bulk separates of cores and rims analyzed by conventional techniques. The shaded region denotes the relatively grossular-rich core.

20. Fluorine microanalyses were done with a 0.5-nA $^{16}O^-$ primary beam focused onto a spot 20 μm in diameter. Negative secondary ions with 50 ± 20 eV excess kinetic energy were detected. The $^{19}F^-$ count rate was normalized to the count rate for ^{18}O, and this ratio was calibrated against Durango apatite. Previous studies in this lab show small matrix effects (≈15%) for F over a range of phases, presumably because F is nearly completely ionized during sputtering [P. Williams, in *Practical Surface Analysis*, D. Briggs and M. P. Seah, Eds. (Wiley, New York, 1992), pp. 177–228]. Error of measurements is within the size of the circles.
21. Rare earth element analyses by ion microprobe were done with the duoplasmatron source to generate a ~1.5-nA ^{16}O primary ion beam at 12.5 kV focused onto a spot 20 μm in diameter. Positive secondary ions of ^{42}Ca, ^{139}La, ^{140}Ce, ^{143}Nd, ^{147}Sm, and ^{166}Er with 75 ± 20 eV excess energy were detected. Erbium contents were corrected for oxides of Nd and Sm, and concentrations were determined according to the methods described by E. Zinner and G. Crozaz [*Int. J. Mass. Spectrom. Ion. Proc.* **69**, 17 (1986)]. Errors (1 SD) of individual measurements were determined by counting statistics. Data tables are available from the authors on request.
22. A. J. Kemp, A. J. Lewis, M. R. Palmer, in preparation.
23. Neodymium isotope data were obtained at the Mineralogical-Geological Museum in Oslo. Isotopic ratios were measured on a VG 354 5-collector fully automated mass spectrometer. Analytical methods follow the procedures described by E. W. Mearns [*Lithos* **19**, 269 (1986)].
24. B. Jamtveit, unpublished results.
25. We thank K. V. Ragnarsdottir for help with the ICP analyses and J. Blundy, K. V. Ragnarsdottir, and R. Wogelius for comments on the manuscript. Supported by the Norwegian Research Council (440.92/023 and 440.93/011).

20 August 1993; accepted 2 December 1993

Glacial-Interglacial Changes in Moisture Sources for Greenland: Influences on the Ice Core Record of Climate

C. D. Charles, D. Rind, J. Jouzel, R. D. Koster, R. G. Fairbanks

Large, abrupt shifts in the $^{18}O/^{16}O$ ratio found in Greenland ice must reflect real features of the climate system variability. These isotopic shifts can be viewed as a result of air temperature fluctuations, but determination of the cause of the changes—the most crucial issue for future climate concerns—requires a detailed understanding of the controls on isotopes in precipitation. Results from general circulation model experiments suggest that the sources of Greenland precipitation varied with different climate states, allowing dynamic atmospheric mechanisms for influencing the ice core isotope shifts.

A network of ice cores now spans much of the Greenland ice sheet. The $\delta^{18}O$ records from the ice cores reveal a pattern of pronounced, abrupt shifts prior to the Holocene period (*1*). The fact that many shifts can be traced among different cores makes it clear that these oscillations are not merely artifacts of local ice sheet dynamics. Yet, their climatic implications have not been fully resolved. Comparison with the $\delta^{18}O$-temperature correlation established from modern precipitation (*2*) implies that the $\delta^{18}O$ shifts, in some cases, reflect temperature fluctuations of 7° to 10°C occurring over the course of less than 20 years (*3*). Obvious questions arise from this type of inference: (i) What aspects of the climate system are capable of creating such large temperature fluctuations over such a broad area and so rapidly? (ii) Can such temperature shifts be triggered in the modern climate through anthropogenic influences?

These oscillations in $\delta^{18}O$ are usually considered to be driven primarily by the North Atlantic because experiments with a coupled ocean-atmosphere model suggest that the North Atlantic thermohaline circulation, which delivers heat to the high latitudes, could alternate between two stable modes of operation (on or off), and aspects of North Atlantic deep-sea sediment records exhibit this type of behavior (*4*). However, several observations also suggest the involvement of other climatic processes. In a series of model experiments that effectively tested the sensitivity of climate to reduced North Atlantic heat transport, this mechanism could explain less than one-third the magnitude of air temperature change over Greenland inferred from the ice core isotopic shifts (*5*). Recent estimation of the rapidity of the changes in the ice cores (*6*) suggests that the variations occur more rapidly than do variations in European climate records that are undeniably the product of North Atlantic surface ocean changes (*7*). New dating of the ice core record at Summit suggests that two of the most prominent $\delta^{18}O$ shifts occur precisely during catastrophic melting of the ice sheets, at about 14,000 and 11,000 years ago (*8*). Thus, it seems unlikely that the North Atlantic acted alone to shape the dramatic ice core records.

To comprehend the full climatic significance of the $\delta^{18}O$ events, we must establish the driving forces for isotopic variability in precipitation. Although the fractionation of $H_2{}^{18}O$ between water vapor and condensate is temperature dependent, the amount of $H_2{}^{18}O$ in precipitation at any given location is more directly determined by the amount of original vapor remaining in the air mass (*9*). Because colder air holds less water vapor, this distillation process also depends on temperature, but the correlation between $\delta^{18}O$ and temperature varies according to the location of the original moisture sources (whether it is remote or proximal), the trajectories of the moisture (whether it is advected along a cold or warm path), and the mixing between sources with different degrees of distillation. Thus, local $\delta^{18}O$ variability may result from a combination of direct air-temperature effects and complicated air mass mixing effects. These influences must be separated for accurate paleoclimatic reconstruction. More importantly, regardless of how the modern $\delta^{18}O$-temperature calibrations apply to the rapid shifts observed in the ice cores (*10*), the causes of the shifts cannot be deduced from empirical extrapolations. One must also understand where and how the characteristics of moisture sources changed under different climate conditions.

One approach is to use a general circulation model (GCM) that is capable of considering explicitly the complex variety of processes that act on the isotopes. Previous GCM studies indicated that although

C. D. Charles, Scripps Institution of Oceanography, University of California at San Diego, La Jolla, CA 92093.
D. Rind, Goddard Institute for Space Studies, New York, NY 10028.
J. Jouzel, Laboratoire de Modelisation du Climat et de l'Environnement, CEA/DSM CE Saclay, 91191 Gif Sur Yvette, France, and Laboratoire de Glaciologie et Geophysique de l'Environnement, CNRS BP96,38402, Saint Martin d'Heres Cedex, France.
R. D. Koster, Hydrological Sciences Branch, National Aeronautics and Space Administration/Goddard Space Flight Center, Greenbelt, MD 20904.
R. G. Fairbanks, Lamont-Doherty Earth Observatory, Palisades, NY 10964, and Department of Geological Sciences, Columbia University, New York, NY 10025.